Imaging Purple Membranes in Aqueous Solutions at Sub-Nanometer Resolution by Atomic Force Microscopy

Daniel J. Müller,*‡ Frank A. Schabert,‡ Georg Büldt,* and Andreas Engel‡

‡M. E. Müller-Institute for Microscopic Structural Biology, Biozentrum, University of Basel, CH-4056 Basel, Switzerland;
*Forschungszentrum Jülich, IBI-2: Structural Biology, D-52425 Jülich, Germany

ABSTRACT   Purple membranes adsorbed to mica were imaged in buffer solution using the atomic force microscope. The hexagonal diffraction patterns of topographs from the cytoplasmic and the extracellular surface showed a resolution of 0.7 and 1.2 nm, respectively. On the cytoplasmic surface, individual bacteriorhodopsin molecules consistently exhibited a distinct substructure. Depending on the pH value of the buffer solution, the height of the purple membranes decreased from 5.6 nm (pH 10.5) to 5.1 nm (pH 4). The results are discussed with respect to the structure determined by cryo-electron microscopy.

INTRODUCTION

The applicability of atomic force microscopy (AFM) (Binnig et al., 1986) for imaging biological molecules in their native environment has been demonstrated shortly after the invention of this technique (Drake et al., 1989). More recently, high-resolution images of two-dimensional (2-D) protein crystals (Butt et al., 1990; Hoh et al., 1993; Karrasch et al., 1994; Schabert and Engel, 1994) and of densely packed proteins (Yang et al., 1993, 1994a,b) have demonstrated that the AFM has become a successful tool which complements other structural techniques such as NMR, x-ray crystallography, and electron microscopy. These results foster the hope that the AFM will allow not only imaging and manipulation of biological surfaces (Hoh et al., 1993), but also direct monitoring of conformational changes of proteins.

Bacteriorhodopsin is a light-driven proton pump in the cell membrane of *Halobacterium salinarium*. The densely packed bacteriorhodopsin molecules form highly ordered 2-D trigonal lattices in the membrane, termed purple membrane for its color. The structural analysis by cryo-electron microscopy has revealed a retinal embedded in seven closely packed α helices (Henderson et al., 1990). A similar arrangement of seven α helical membrane spanning segments has also been observed for halorhodopsin (Havelka et al., 1993) and rhodopsin (Schertler et al., 1993). Moreover, this feature represents the common motif of the G protein-coupled receptor family (Baldwin, 1993). Comparing recent AFM studies of purple membrane, a continuous improvement of the AFM image quality of crystals becomes evident (Worcester et al., 1988, 1990; Butt et al., 1990, 1991, 1992). In this paper we demonstrate that submolecular details of single bacteriorhodopsin molecules can be resolved and interpreted with

respect to the atomic model derived from electron microscopy (Henderson et al., 1990).

MATERIALS AND METHODS

Specimen preparation

Purple membranes of *Halobacterium salinarium* strain ET1001 were isolated as described by Oesterhelt and Stoeckenius (1974). The membranes were frozen and stored at −70°C. Thawed samples were kept at 4°C before adsorption to mica and viewing in the AFM.

Purple membrane stock solution (10 mg/ml in double distilled water) was diluted 200-fold in the respective sample buffer. A 25-μl drop of this solution was deposited on freshly cleaved mica discs (10 mm in diameter) that had been glued onto 25 mm Teflon discs fixed to magnetic holders (Schabert and Engel, 1994). After 10 to 30 min, the sample was gently washed with buffer to remove membranes that were not firmly attached to the substrate. The pH was adjusted between 3 and 5 (10 mM citric acid), 5 and 6 (10 mM Mes), 6 and 8 (10 mM HEPES) and 8 and 10.5 (10 mM Tris). All four buffers contained 150 mM KCl. In addition, Tris-KCl buffer was supplemented with 1 mM EDTA or with 2 or 20 mM $MgCl_2$ where indicated.

Alternatively, the freshly cleaved mica was coated with polylysine hydrobromide (M_r 2200–4000; Sigma, 9470 Buchs, Switzerland) by applying an aqueous solution at a concentration of 10 mg/ml for 1 min, washing gently with water, and allowing to dry in air or in a stream of N_2. Purple membranes were adsorbed under illumination by light to favor one orientation of membrane attachment (Fisher et al., 1978).

Instrumentation and operation of the AFM

A commercial AFM (Nanoscope III, Digital Instruments, Santa Barbara, CA) equipped with a 15-μm scanner (d-scanner) and a liquid cell was used. The 120 μm long cantilevers with a nominal force constant of k = 0.38 N/m and oxide sharpened Si_3N_4 tips were purchased from Digital Instruments. The liquid cell was used without an O-ring seal. After several hours of thermal relaxation, the drift of the cantilever deflection angle corresponded to $\sim$0.3 nm per min. Initial engagement of the tip was performed by setting the scanning size to 0 to minimize specimen deformation or tip contamination. Before scanning the surfaces, the operating point of the microscope was set to forces below 1 nN.

At low magnification (frame size $\sim$600 nm) imaging was performed in the error signal mode acquiring the deflection and height signal simultaneously. The deflection signal was minimized by optimizing gains and scan speed. The scan speed was roughly linear to the scan size, 4 to 8 lines per second for lower magnifications (frame size 0.35–13 μm) and 8 to 9.6 lines per second for higher magnifications (frame sizes 80–130 nm). Thus, for high-resolution imaging the maximum speed (1.25 μm/s) was below the critical scan speed of $\sim$2 μm/s (Butt et al., 1993). At high magnification,

the deformation of the sample was monitored by comparing the height profiles acquired in trace and retrace direction and at different scan angles. The applied force was corrected manually to compensate for the thermal drift of the microscope.

For image processing, all raw data were transferred to a Vax 3100 workstation and analyzed using the Semper image processing system (Saxton, 1979) from Synoptics Ltd., Cambridge, UK. Images were flattened line by line, and correlation averaged as described (Schabert and Engel, 1994).

Calibration of the scanner was carried out using layered crystals such as mica (Bailey, 1984) and transition metal dichalcogenides (Wilson and Yoffe, 1963) as substrate references. The lateral calibration was carried out by comparing the lattice constants of the layered surface, and for calibration in z-direction, defects (large holes or steps) were used (Jungblut et al., 1992). The height variations of these surface defects represent multiples of the thickness of a single crystal layer including the respective van der Waals gap.

RESULTS AND DISCUSSION

Adsorption and height of purple membranes deposited on freshly cleaved mica in dependence of salts and pH

Fig. 1 shows a typical overview (frame size 12 μm) of purple membranes adsorbed to freshly cleaved mica at pH 9. Membrane sheets up to a diameter of 2 μm remained flatly adsorbed to the substrate and remained stable during several hours of scanning. At 150 mM KCl, the formation of stacks was rarely observed. Below pH values of 3.8, the majority of the membranes were poorly adsorbed and aggregated within 30 min. However, purple membranes were more stable and imaging was possible at pH 3 if the KCl concen-

tration was increased to 500 mM. At pH values above 9.2, some of the membrane sheets slowly aggregated within 12–24 h. The pH of the buffer solution also affected the height of adsorbed purple membranes. Averages of at least 150 height measurements on membranes that were flatly adsorbed to the mica surface at different pH values are plotted in Fig. 2. As indicated by the horizontal line, the height of the membranes at pH values above 6 is 5.6 ± 0.1 nm. Below pH 6, the height continuously decreases to reach a plateau of 5.1 ± 0.1 nm at pH 4. A similar value (5.0 nm) was measured for the lamellar spacing of dried purple membrane stacks by low angle x-ray scattering (Blaurock and Stoeckenius, 1971).

Our height data also correlate with the pH dependence of the lamellar spacings (Henderson, 1975). In the latter work, the spacings of the purple membranes were measured after drying on mica at different pH values. At pH 10, the repeat was 5.3 nm, decreasing to 4.86 nm at pH 4. The difference of 0.44 nm is in good agreement with the height difference of 0.5 nm that we determined by AFM, despite the different experimental conditions. Furthermore, it is interesting to note that the bacteriorhodopsin structure derived from electron crystallographic data of purple membranes prepared at pH 5.2 exhibits a height of 4.9 ± 1.0 nm (Henderson et al., 1990).

It is surprising that in spite of the lipids the most prominent changes in height occur at pH values near the isoelectric point pI of solubilized bacteriorhodopsin (5.2; Ross et al., 1989). This led us to speculate that electrostatic forces may play a major role in the conformation of the loops connecting the α-helices. Thus, charge neutralization may result in the observed height alterations. Furthermore, the increasing proton concentration may compensate the negative surface charge of the mica (Bailey, 1984). However, it is difficult to assess the resulting force from all the different types of forces acting between the substrate and the membrane. Thus, further experiments are necessary to explain the observed pH dependence of the membrane height in depth.

It has been reported by Butt et al. (1990, 1991) that divalent cations may mediate the adsorption of purple membrane to mica. However, the adsorption behavior was unchanged in the presence of 1 mM EDTA, suggesting that divalent ions are not responsible for the adsorption mecha-
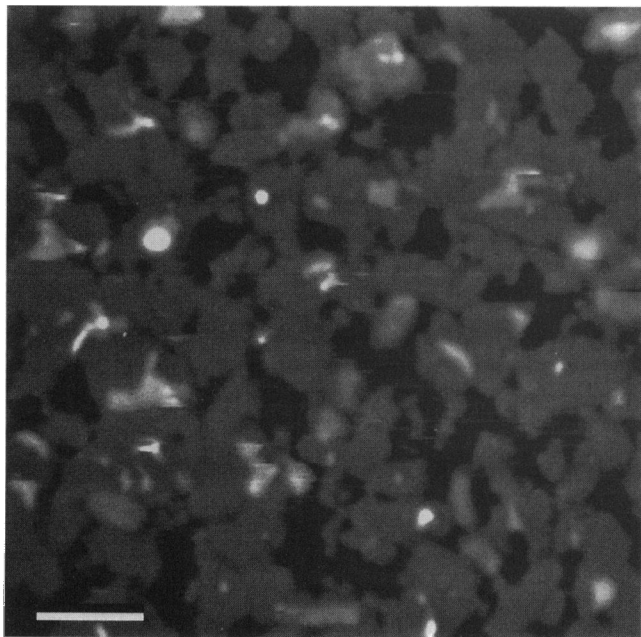

FIGURE 1 AFM image of purple membranes adsorbed to mica in the presence of 150 mM KCl. No overlapping or stacking of the membranes was observed for pH values between 4 and 10 as demonstrated by this densely covered surface prepared at pH 9. The average height of these membranes was 5.6 nm. Scale bar = 2 μm.
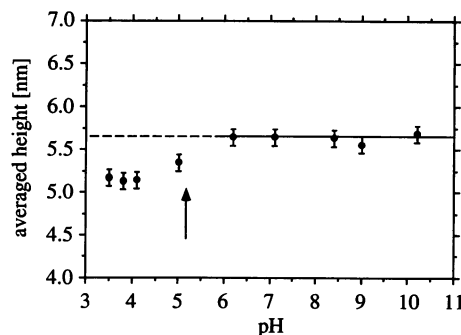

FIGURE 2 Height of purple membranes adsorbed to mica versus pH. For each point the average of 150 membranes was calculated. The arrow indicates the isoelectric point of bacteriorhodopsin.

nism. To test whether KCl is a crucial determinant, experiments using low salt buffers devoid of monovalent salts were carried out. When scanning areas of 18 μm side length, we occasionally detected a membrane sheet and some large aggregates at best. Apparently, the binding to freshly cleaved mica was weak in the absence of KCl and the membranes were readily displaced by the stylus. Addition of 2 or 20 mM $MgCl_2$ to the KCl buffer or replacing K^+ by Na^+ diminished the adsorption as well.

These observations suggest that divalent cations are less efficient than monovalent ions, in particular K^+, for the adsorption of purple membrane to freshly cleaved mica. It appears that the interactions between mica and membrane are not only of electrostatic nature, but that other forces should be considered. In fact, purple membranes adsorbed surprisingly well to highly ordered pyrolitic graphite and to silanized surfaces using the buffers specified in Materials and Methods supplemented with 150 mM KCl.

High-resolution imaging of bacteriorhodopsin molecules

An intermediate magnification image (frame size 360 nm) of a purple membrane is shown in Fig. 3. The membrane was adsorbed to mica and imaged at pH 8.2, revealing highly ordered "donut"-like protrusions, which represent the bacteriorhodopsin trimers arranged in a trigonal lattice. While the lattice constant of 6.2 $\pm$ 0.2 nm agrees with data from
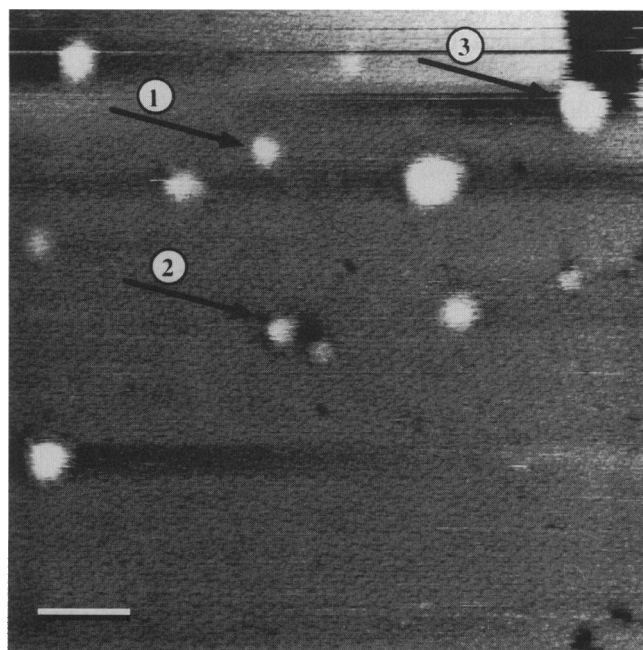

FIGURE 3   AFM image of a purple membrane recorded at pH 8.2. The hexagonal array of donut-like protrusions is distinct. Bumps, that formed during scanning are seen in different stages. Stage one (*arrow 1*) shows the bending of the surface. During stage two (*arrow 2*) the membrane was disrupted. The debris were displaced by the tip, and eventually settled at the edge of the 2-D crystal (*arrow 3*). The scale bar represents 50 nm, and the gray level range extends over 3 nm.

electron crystallography (Henderson and Unwin, 1975), the angle between the lattice vectors frequently deviated from the expected 60°C as a result of thermal drift. In the presence of 150 mM KCl, topographs exhibiting submolecular resolution with a high signal-to-noise (S/N) ratio were more frequently recorded at pH values above 8 than at neutral pH. As illustrated by Fig. 3, the formation of bumps with diameters between 10 and 30 nm could be monitored over several scans until the membrane ruptured and the resulting debris were pushed away by the tip. The displaced aggregates frequently settled at the edges of the membranes. The formation of the bumps may be the result of adsorbates that prevented the attractive interaction between membrane and substrate.

At high magnification (frame size 137 nm), bacteriorhodopsin trimers revealed a distinct donut-like shape (Fig. 4 *a*). The membranes were adsorbed and imaged at pH 9.2 (150 mM KCl). The power spectrum (Fig. 4 *b*) exhibits diffraction orders up to a resolution of 0.7 nm. Although the appearance of the donuts varies considerably, their tripartite morphology is evident in the unprocessed sum of trace and retrace scan (Fig. 4 *a*). As documented by the unsymmetrized average of $\sim$200 unit cells (Fig. 4 *c*), the donuts appear to be connected with fibrous arms. Combining averages from four independent images, the tripartite structure becomes more distinct (root-mean-square (RMS) deviation from the threefold symmetry: 4.6%), but the connecting arms exhibit less contrast (Fig. 4 *d*). The appearance does not change significantly after threefold symmetrization (Fig. 4 *e*). The corrugation amplitude of averaged and symmetrized unit cells of four images recorded with different tips was 0.41 $\pm$ 0.025 nm. All averaged topographs exhibited bacteriorhodopsin monomers with two domains of comparable height above the lipid surface (0.41 nm) which were 1.45 $\pm$ 0.1 nm apart. The two domains were arranged on circles with radii of 1.47 $\pm$ 0.1 and 1.67 $\pm$ 0.1 nm, respectively. As a result of this, different distances between inner domains (2.65 $\pm$ 0.1 nm) and outer domains (2.89 $\pm$ 0.1 nm) dominated the topography.

Purple membrane adsorbed to polylysine-coated mica

To determine the orientation of the membranes displayed in Figs. 3 and 4, we adopted the experimental procedure described by Hayward et al. (1978) and Fisher et al. (1978). They observed that purple membranes adsorbed to polylysine-coated surfaces in different orientations depending on the pH value. At pH 7.4, 92% of the membranes were attached with the cytoplasmic side to the polylysine, whereas at pH 3 more than 95% of the membranes were attached with their extracellular side (Fisher et al., 1977).

The polylysine-coated mica surface had a surface roughness of $\sim$1.1 nm (Fig. 5 *a*). Purple membranes were deposited on the polylysine- treated mica at pH 4, 5.5, 7.4, 9, and 10.5 in the presence of 150 mM KCl. As demonstrated in Fig. 5, *b* and *c*, purple membranes adsorbed differently to the polylysine-coated mica at different pH values. The ratio of "bright" to "dark" membranes increased from $\sim$0.1 at pH 7.4
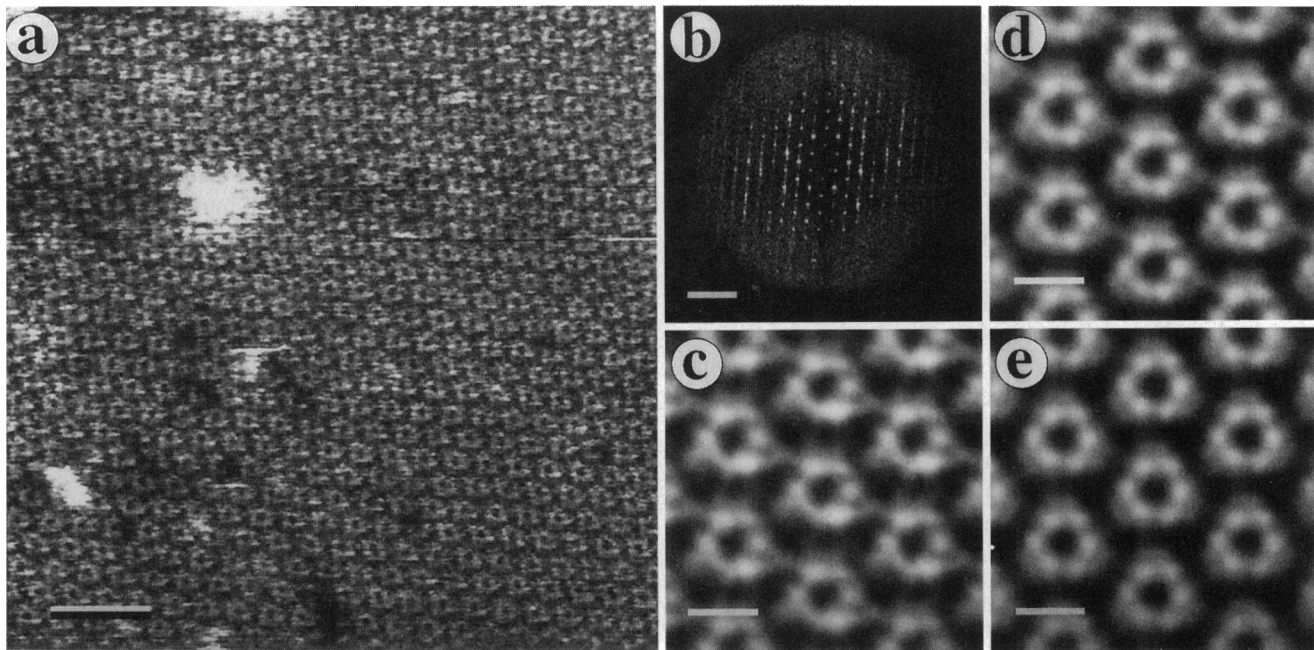
FIGURE 4   High-resolution AFM topograph of the same purple membrane surface as shown in Fig. 3. (a) The bacteriorhodopsin trimers reveal reproducible substructure. (b) To display weak diffraction orders that were significantly higher than the background, the diffraction pattern has been weighted with a radial ramp. Diffraction orders extend beyond a resolution of 0.7 nm; their splitting is the result of a distortion along the slow scan direction. (c) The correlation average of ~200 unit cells exhibited a RMS deviation from threefold symmetry of 14%, and has a height of 0.49 nm. (d) The average from four independent images has a RMS deviation from threefold symmetry of 4.6%. (e) After threefold symmetrization its height is 0.41 nm. Scale bars represent 20 nm in the image, 4 nm in the averages, and $(2 \text{ nm})^{-1}$ in the diffraction pattern.
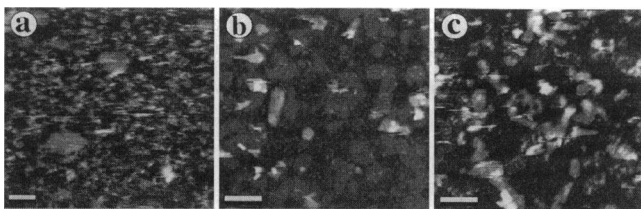

FIGURE 5   Purple membrane adsorbed to polylysine-coated mica. (a) The polylysine forms structures of various shapes and dimensions when deposited on freshly cleaved mica and dried in a nitrogen stream. The topograph was recorded in 150 mM KCl adjusted to pH 7.8 and had a corrugation of 1.1 nm. (b) Purple membranes adsorbed to polylysine-coated mica predominantly as single layers at pH values above 7. (c) At pH 5.5, a major fraction of the adsorbed membranes had a height above 11 nm. Scale bars represent 100 nm in (a), 1 μm in (b) and (c). The gray level corresponds to 10 nm in (a) and 50 nm in (b) and (c).

to >1 at pH 5.5. At low magnification "bright" membranes were swept away by the tip at forces of 1 nN. Their height varied between 10 nm and 16 nm, suggesting that "bright" membranes may represent stacks of two or three purple membranes.

Although the single-layered membranes adsorbed well to polylysine treated mica at all pH values, it was more difficult to achieve high resolution than without polylysine. The topographs exhibited a lower S/N ratio than those of Figs. 3 and 4, while power spectra showed orders up to 1.2 nm resolution at pH 9 (Fig. 6, a and b). As documented by Fig. 6 c, the membranes were not flat and the lattice was distorted. We

attribute this to the roughness of the polylysine-covered surface which in turn may lead to a buckling of the purple membrane. Nevertheless, correlation averages of membranes recorded at pH 9 exhibited a tripartite morphology (Fig. 6 d) that was enhanced by threefold rotational symmetrization (Fig. 6 e). The corrugation amplitude of this topography was 0.15 ± 0.02 nm ($n = 3$), and the disposition of the protrusions was different compared to the topography shown in Fig. 4. The unit cell exhibited three domains surrounding one three-fold axis and a single protrusion about another threefold axis.

In analogy to the findings reported by Fisher et al. (1978) and Hayward et al. (1978) we tentatively attribute the unit cell surface topography shown in Fig. 6 to the extracellular side. Therefore, the distinct topographs of the membranes adsorbed to uncoated mica (Figs. 3 and 4) may represent the cytoplasmic surface.

Comparison with the purple membrane structure determined by electron crystallography

Previous AFM studies did not allow identification of the surface (Butt et al., 1990, 1991), whereas an electron microscopic analysis of heavy metal decorated purple membranes indicated that the rough surface corresponds to the extracellular side (Studer et al., 1981). With the latter technique the apparent surface texture reflects the disposition of the sites decorated by metal clusters rather than the actual physical surface corrugation (Neugebauer and Zingsheim, 1978). Therefore, our finding that the presumed cytoplasmic
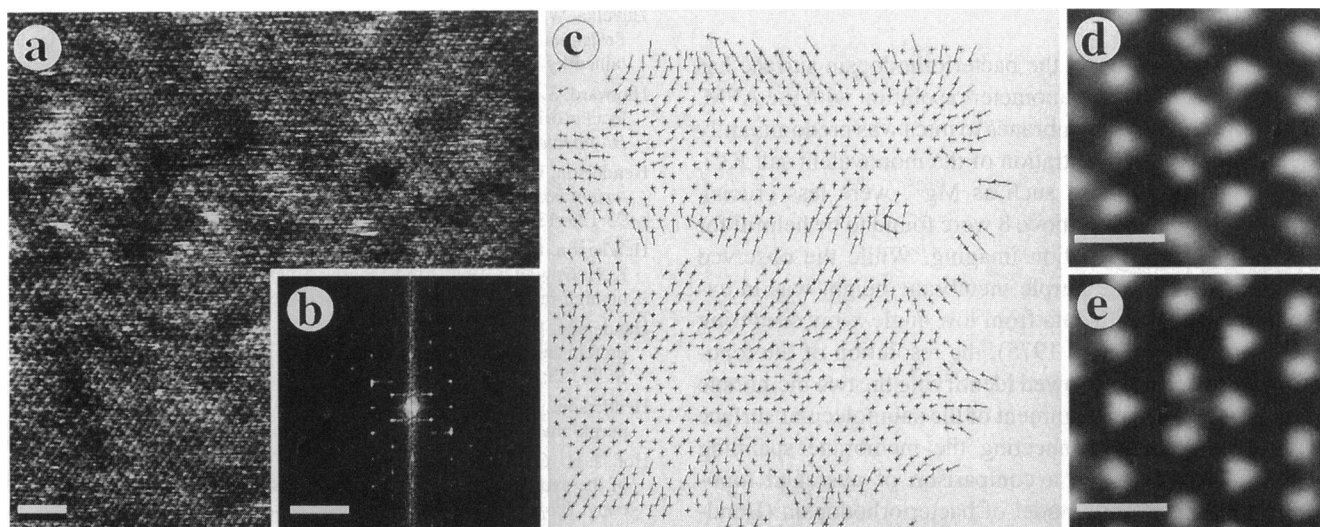
FIGURE 6   Single layered purple membrane adsorbed to polylysine-coated mica at neutral pH showed a hexagonal pattern. (a) Compared to the membranes shown in Figs. 3 and 4, they were less flat as a result of the polylysine. (b) Nevertheless, diffraction orders extending to a resolution of 1.18 nm are visible in the diffraction pattern. (c) The lattice disorder is demonstrated by the displacement map. Vectors emanating from the unit cell positions toward the nearest fitted lattice point are fivefold magnified. (d) The correlation average deviated from threefold symmetry by 20%, and the symmetrized surface map (e) has a height of 0.14 nm. Scale bars represent 20 nm in (a), (2 nm)$^{-1}$ in (c), and 4 nm in (d).

surface of bacteriorhodopsin protrudes almost 3 times further from the bilayer surface than the extracellular surface is not in contradiction with the results of Studer et al. (1981). In addition, we need to consider the possibility that the stylus senses the carbohydrates of the glycolipids, which represent the majority of lipids in the extracellular leaflet of the bilayer (Henderson et al., 1978).

It is tempting to compare the various inter domain distances with the bacteriorhodopsin structure from electron crystallography (Unwin and Henderson, 1975; Henderson and Unwin, 1975; Henderson et al., 1990). In Fig. 7 this structural information is superimposed on the features of the combined average from five images of the cytoplasmic surface. While the domains of the outer circle are remarkably close to the B helices of the bacteriorhodopsin molecules, the domains of the inner circle are more difficult to interpret. Their position is close to the loop connecting helices C and D. As this loop is short, we propose that the inner domains may rather represent the most prominent loop at the cytoplasmic surface which connects helices E and F. In this case, loop E-F would be shifted by ~0.8 nm toward the center of the trimer, which could be the result of a tip-induced conformational change. Experiments to prove this interpretation are currently in progress.

Compared to the resolution of the cytoplasmic surface (0.7 nm; Fig. 4), the resolution of the trimeric structure (1.2 nm; Fig. 6) on the extracellular surface is lower. Therefore, the most prominent loops on the extracellular surface connecting helices B-C and F-G, which are 1.2 nm apart, cannot be resolved. However, these loops could have produced the single protrusions characteristic for each bacteriorhodopsin molecule. This interpretation is consistent with the atomic model of bacteriorhodopsin (Henderson et al., 1990), which exhibits a distance of 3.2 nm between the centers of mass of
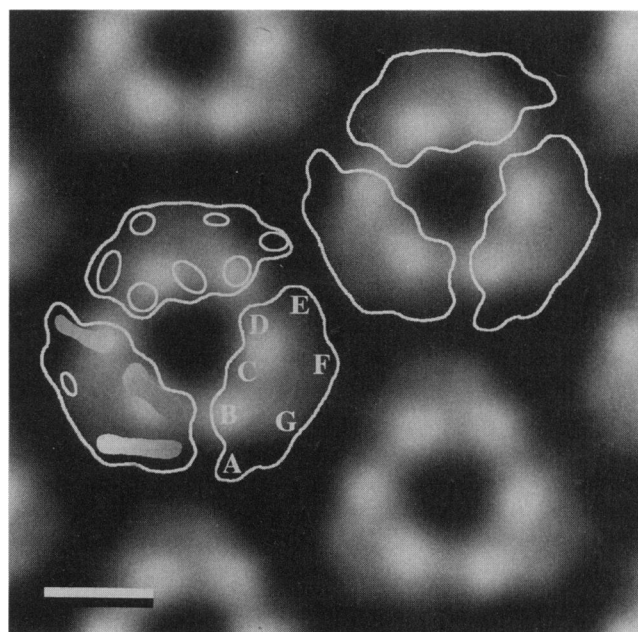

FIGURE 7   Averaged and threefold symmetrized topography of the cytoplasmic surface calculated from five images recorded with different tips. Similar to the average displayed in Fig. 4, the bacteriorhodopsin molecules are divided into two domains. Contours delineating the bacteriorhodopsin molecules in the upper right trimer and the α helices in the left trimer are from the projection map determined by electron crystallographic methods (Unwin and Henderson, 1975). The lower left diagram shows the loops connecting the helices at the cytoplasmic surface according to the three-dimensional atomic model (Henderson et al., 1990), with high protrusions in bright shades. The C-terminal end of the molecule is located at the cytosolic end of helix G. Scale bar = 2 nm.

loops B-C and F-G, as well as a slight clockwise rotation of the trimer. Thus, the centers are close to the position of the protrusions observed by AFM.

CONCLUSIONS

Structural information of the bacteriorhodopsin surface has been acquired with sub-nanometer resolution with the AFM. The adsorption of the membranes to mica was predominantly influenced by the concentration of the monovalent salt KCl, whereas divalent cations such as Mg^{2+} were less crucial. Furthermore, pH values above 8 were found to be helpful for reproducible high-resolution imaging. While the observed pH dependence of the purple membrane height was in excellent agreement with data from low angle x-ray scattering experiments (Henderson, 1975), the resolution of the topographs presented here allowed identifying the two membrane surfaces. A tentative assignment of the submolecular surface corrugation to loops connecting the membrane spanning α-helices emerged from a comparison of averaged topographs with the atomic model of bacteriorhodopsin (Henderson et al., 1990).

REFERENCES

Bailey, S. W. (Editor). 1984. Micas. In Review of Minerals, Vol. 13.

Baldwin, J. M.. 1993. The probable arrangement of the helices in G protein-coupled receptors. EMBO J. 12:1693–1703.

Binnig, G., C. F. Quate, and C. Gerber. 1986. Atomic force microscope. Phys. Rev. Lett. 56:930–933.

Blaurock, A. E., and W. Stoeckenius. 1971. Structure of the purple membrane. Nature New Biol. 233:152–155.

Butt, H.-J., K. H. Downing, and P. K. Hansma. 1990. Imaging the membrane protein bacteriorhodopsin with the atomic force microscope. Biophys. J. 58:1473–1480.

Butt, H.-J., R. Guckenberger, and J. P. Rabe. 1992. Quantitative scanning tunneling microscopy and scanning force microscopy of organic crystals. Ultramicroscopy. 46:375–393.

Butt, H.-J., C. B. Prater, and P. K. Hansma. 1991. Imaging purple membranes dry and in water with the atomic force microscope. J. Vac. Sci. Technol. B9:1193–1196.

Butt, H.-J., P. Siedle, K. Seifert, K. Fendler, T. Seeger, E. Bamberg, A. L. Weisenhorn, K. Goldie, and A. Engel. 1993. Scan speed limit in atomic force microscopy. J. Microsc. 169:75–84.

Drake, B., C. B. Prater, A. L. Weisenhorn, S. A. C. Gould, T. R. Albrecht, C. F. Quate, D. S. Cannell, H. G. Hansma, and P. K. Hansma. 1989. Imaging crystals, polymers, and processes in water with the atomic force microscope. Science. 243:1586–1588.

Fisher, K. A., K. Yanagimoto, and W. Stoeckenius. 1977. Purple membrane bound to polylysine glass: effects of pH and light. J. Cell. Biol. 75:200a.

Fisher, K. A., K. Yanagimoto, and W. Stoeckenius. 1978. Oriented adsorption of purple membrane to cationic surfaces. J. Cell Biol. 77:611–621.

Havelka, W. A., R. Henderson, J. A. W. Heymann, and D. Oesterheldt. 1993. Projection structure of Halobacterium halobium at 6 Å resolution obtained by electron cryo-microscopy. J. Mol. Biol. 234:837–846.

Hayward, S. B., D. A. Grano, R. M. Glaeser, and K. A. Fisher. 1978. Molecular orientation of bacteriorhodopsin within the purple membrane of Halobacterium halobium. Proc. Natl. Acad. Sci. USA. 75:4320–4324.

Henderson, R. 1975. The structure of the purple membrane from Halobacterium halobium: analysis of the x-ray diffraction pattern. J. Mol. Biol. 93:123–138.

Henderson, R., J. M. Baldwin, T. A. Ceska, F. Zemlin, E. Beckmann, and K. H. Downing. 1990. Model for the structure of bacteriorhodopsin based on high-resolution electron cryo-microscopy. J. Mol. Biol. 213:899–929.

Henderson, R., J. S. Jubb, and S. Whytock. 1978. Specific labeling of the protein and lipid on the extracellular surface of purple membrane. J. Mol. Biol. 123:259–274.

Henderson, R., and P. N. T. Unwin. 1975. Three-dimensional model of purple membrane obtained by electron-microscopy. Nature. 257:28–32.

Hoh, J. H., G. E. Sosinsky, J.-P. Revel, and P. K. Hansma. 1993. Structure of the extracellular surface of the gap junction by atomic force microscopy. Biophys. J. 65:149–163.

Jungblut, H., S. A. Campbell, M. Giersig, D. J. Müller, and H.-J. Lewerenz. 1992. Scanning tunneling microscopy observations of biomolecules on layered materials. Faraday Discuss. 94:183–198.

Karrasch, S., R. Hegerl, J. Hoh, W. Baumeister, and A. Engel. 1994. Atomic force microscopy produces faithful high-resolution images of protein images in an aqueous environment. Proc. Natl. Acad. Sci. USA. 91:836–838.

Neugebauer, D.-C., and H. P. Zingsheim. 1978. The two faces of the purple membrane. J. Mol. Biol. 123:235–246.

Oesterhelt, D., and W. Stoeckenius. 1974. Isolation of the cell membrane of Halobacterium halobium and Its fractionation into red and purple membrane. Methods Enzymol. 31:667–678.

Ross, P. E., S. L. Helgerson, L. J. W. Miercke, and E. A. Dratz. 1989. Isoelectric focusing studies of bacteriorhodopsin. Biochim. Biophys. Acta 991:134–140.

Saxton, W. O., T. J. Pitt, and M. Horner. 1979. Digital image processing: the semper system. Ultramicroscopy. 4:343–354.

Schabert, F., and A. Engel. 1994. Reproducible acquisition of E. coli porin surface topographs by atomic force microscopy. Biophys. J. 67:2394–2403.

Schertler, G. F. X ., D. Villa, and R. Henderson. 1993. Projection structure of rhodopsin. Nature. 362:770–772.

Studer, D., H. Moor, and H. Gross. 1981. Single bacteriorhodopsin molecules revealed on both surfaces of freeze-dried and heavy metal-decorated purple membranes. J. Cell Biol. 90:153–159.

Unwin, P. N. T., and R. Henderson. 1975. Molecular structure determination by electron microscopy of unstained crystalline specimens. J. Mol. Biol. 94:425–440.

Wilson, J. A., and A. D. Yoffe. 1963. The transition metal dichalcogenides. Adv. Phys. 18:193–335.

Worcester, D. L., H. S. Kim, R. G. Miller, and P. J. Bryant. 1990. Imaging bacteriorhodopsin lattices in purple membranes with atomic force microscopy. J. Vac. Sci. Technol. A8:403–405.

Worcester, D. L., R. G. Miller, and P. J. Bryant. 1988. Atomic force microscopy of purple membranes. J. Microsc. 152:817–821.

Yang, J., J. Mou, and Z. Shao. 1994a. Molecular resolution atomic force microscopy of soluble proteins in solution. Bba 1199:105–114.

Yang, J., J. Mou, and Z. Shao. 1994b. Structure and stability of pertussis toxin studied by in situ atomic force microscope. FEBS Lett. 338:89–92.

Yang, J., L. K. Tamm, T. W. Tillak, and Z. Shao. 1993. New approach for atomic force microscopy of membrane proteins. J. Mol. Biol. 229:286–290.